iScience

CellPress
OPEN ACCESS

Article

Identifying signatures of EV secretion in metastatic breast cancer through functional single-cell profiling

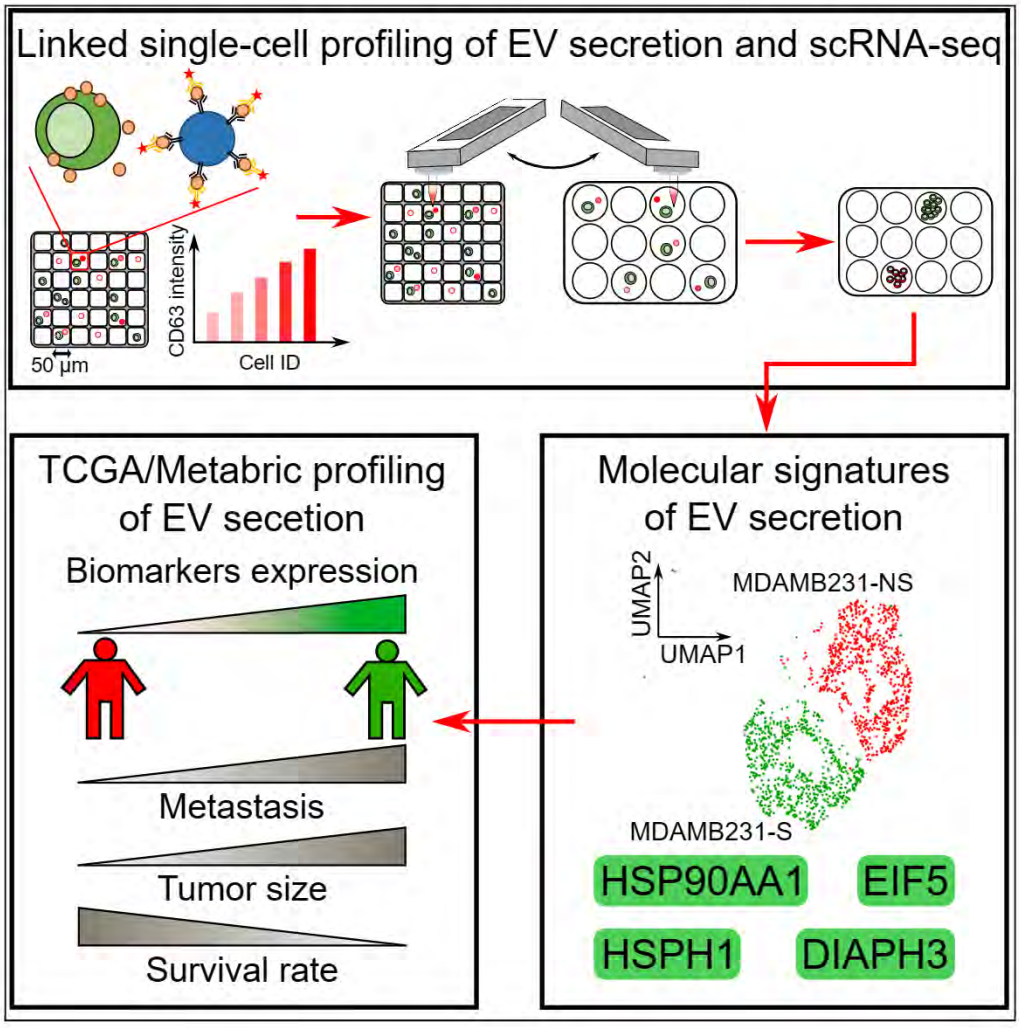

Mohsen Fathi, Melisa Martinez-Paniagua, Ali Rezvan, ..., Ken Chen, Sendurai A. Mani, Navin Varadarajan

nvaradar@central.uh.edu

Highlights

A novel assay for the integrated profiling of single-cell EV secretion and scRNA-seq

We identified and validated EV-sig a signature of EV secretion in breast cancer

EV-sig is clinically associated with highly invasive cancers and poor survival

Fathi et al., iScience 26, 106482
April 21, 2023
https://doi.org/10.1016/j.isci.2023.106482

iScience

CellPress
OPEN ACCESS

Article

Identifying signatures of EV secretion in metastatic breast cancer through functional single-cell profiling

Mohsen Fathi,[1] Melisa Martinez-Paniagua,[1] Ali Rezvan,[1] Melisa J. Montalvo,[1] Vakul Mohanty,[2] Ken Chen,[2] Sendurai A. Mani,[3,4,5] and Navin Varadarajan[1,6,*]

SUMMARY

Extracellular vesicles (EVs) regulate the tumor microenvironment by facilitating transport of biomolecules. Despite extensive investigation, heterogeneity in EV secretion among cancer cells and the mechanisms that support EV secretion are not well characterized. We developed an integrated method to identify individual cells with differences in EV secretion and performed linked single-cell RNA-sequencing on cloned single cells from the metastatic breast cancer cells. Differential gene expression analyses identified a four-gene signature of breast cancer EV secretion: *HSP90AA1*, *HSPH1*, *EIF5*, and *DIAPH3*. We functionally validated this gene signature by testing it across cell lines with different metastatic potential *in vitro*. Analysis of the TCGA and METABRIC datasets showed that this signature is associated with poor survival, invasive breast cancer types, and poor CD8$^+$ T cell infiltration in human tumors. We anticipate that our method for directly identifying the molecular determinants of EV secretion will have broad applications across cell types and diseases.

INTRODUCTION

Extracellular vesicles (EVs) are a heterogeneous population of lipid bilayers that encapsulate and transport diverse biological cargo including nucleic acids and proteins.[1,2] EVs appear to be secreted from diverse mammalian cell types and are hypothesized to mediate long-range cell-cell communication.[3–5] In the last two decades, it has become evident that EV-mediated transport and delivery of biomolecules is important not only in normal physiological processes but also in pathological processes including cardiovascular disorders and cancers.[6] EVs influence every step of tumor progression and metastasis. Tumor-derived EVs induce upregulation of angiogenesis-related genes and enhance endothelial cell proliferation,[7] facilitate immunosuppression through the transfer of PD-L1,[8] enable invasion through the activity of the matrix metallopeptidase 2 (MMP2)[9] and seed the pre-metastatic niche by downregulating expression of cadherin-17 in lung.[10] Tumor-derived EVs have potential for diagnostic purposes and methods have been developed to dissect the heterogeneity of EVs down to the single particle-level.[11–13]

The pathways that regulate the secretion and packaging of EVs are not completely understood.[14] EVs are classified based on their mode of release as ectosomes or exosomes. Ectosomes, or shedding microvesicles, are released through the outward budding of the plasma membrane. Exosomes, by contrast, are synthesized by the inward budding of the endosomal membrane, which leads to formation of early endosomes. The maturation of early endosomes results in the formation of multivesicular bodies (MVB), and the fusion of the MVBs with the plasma membrane lead to secretion of exosomes. Proteins associated with MVB sorting include components of the endosomal sorting complexes required for transport (ESCRT) complex[15,16]; and ESCRT-independent molecules such as sphingolipid ceramide[17] and tetraspanin CD63.[18] Proteins associated with the fusion of MVBs with the plasma membrane include the SNAREs[19,20] and the ras-associated binding (RAB) family members RAB27A, RAB27B, and RAB7.[21,22] Despite this progress in identifying the molecular components of EV secretion, the map of proteins that participate in EV secretion remains incomplete. Most studies have focused on profiling the cargo of EVs, but this profiling largely reflects information being transferred rather than the molecules responsible for EV secretion.[23,24]

[1]Chemical and Biomolecular Engineering Department, University of Houston, 4726 Calhoun Road, Houston, TX 77204, USA

[2]Department of Bioinformatics and Computational Biology, University of Texas M.D. Anderson Cancer Center, 1400 Pressler Street, Houston, TX, USA

[3]Department of Translational Molecular Pathology, University of Texas M.D. Anderson Cancer Center, 2130 W Holcombe Boulevard, Houston, TX 77030, USA

[4]Department of Pathology and Lab Medicine, Warren Alpert Medical School, Brown University, Providence, RI 02903, USA

[5]Legoretta Cancer Center, Brown University, Providence, RI 021912, USA

[6]Lead contact

*Correspondence: nvaradar@central.uh.edu

https://doi.org/10.1016/j.isci.2023.106482

To directly link secretion of EVs with underlying molecular properties at single-cell resolution, we integrated single-cell EV profiling and cloning with single-cell RNA-sequencing (scRNA-seq) to enable unbiased discovery of the genes that influence EV secretion. We utilized the well-validated metastatic breast cell line, MDAMB2321, which has been known to secrete EVs that enhance migration and invasion of cancer cells.[25] By performing scRNA-seq analysis on individual cells that either secretes high or low amounts of EVs, we discovered a four-gene signature, *HSP90AA1*, *HSPH1*, *EIF5*, and *DIAPH3*, correlated with EV secretion. We experimentally validated this core signature in breast cell lines *in vitro* and confirmed that HSP90 inhibitors negatively regulate EV secretion. Based on analysis of the Cancer Genome Atlas (TCGA), high expression of the EV signature is strongly correlated with poor survival and low $CD8^+$ T cell infiltration in breast cancer patients.

RESULTS

Establishing monoclonal cell lines with heterogeneous EV secretion

To directly analyze EV secretion by clonal cells, we utilized nanowell arrays.[26] We mapped the heterogeneity in EV secretion within the metastatic triple-negative breast cancer cell line, MDAMB231, with the aid of two EV markers known to be expressed in these cells, CD63 and CD81 (Figure 1A). Single-cell profiling demonstrated that individual cells secrete very different amounts of EVs (Figures 1B and S1).[27] To determine whether EV secretion is a stably inheritable property, we retrieved individual EV secretor (labeled MDAMB231-S) and non-secretor cells (MDAMB231-NS) using an automated robot and expanded them to establish clonal populations. After limited expansion (< 20 generations), we evaluated secretion rate by single cells from these clonal populations and confirmed that individual cells from the MDAMB231-S population secreted more EVs than MDAMB231-NS cells at all-time points tested (Figure 1C). Tracking the kinetics of EV secretion showed that the majority (> 87%) of both MDAMB231-S and MDAMB231-NS cells secreted EVs continuously over the 6 h period monitored (Figure 1D). Since EV secretion is associated with increased migration in metastatic breast cancer cells,[28] we compared the migratory potentials of MDAMB231-S and MDAMB231-NS populations using a wound healing assay. The MDAMB231-S cells were significantly more migratory than the MDAMB231-NS cells (Figure 1E). Taken together, these results showed that we can identify cells with differences in EV secretion and that the EV secretion property is maintained upon clonal expansion.

Next, we sought to directly evaluate the effect of EVs secreted by MDAMB231-S and MDAMB231-NS cells (Figure S2A). Accordingly, we isolated the EVs from culture media of MDAMB231-NS and MDAMB231-S cell lines and measured the size distribution and concentration of EVs using nanoparticle tracking analysis (Figures S2B and S2C). We evaluated the effect of isolated EVs ($8x10^8$ particles/ml) on the migration of parental MDAMB231, MDAMB231-S, and MDAMB231-NS cell lines using a standard wound healing assay. The results showed that EVs isolated from MDAMB231-S cells enhanced the migration of parental MDAMB231 and MDAMB231-NS cells, but did not have a significant effect on migration of MDAMB231-S cells (Figures S2D–S2F). These results show that the EVs secreted by MDAMB231-S cells can induce the migration of MDAMB231 cells.

Identification of an EV gene signature in breast cancer cells

The availability of the clonal populations allowed us to compare the transcriptional differences across thousands of single cells by scRNA-seq. To derive a genetic signature associated with EV secretion, we performed scRNA-seq on cells from the MDAMB231-S and MDAMB231-NS populations using the Rhapsody platform (Figure 2A). After data processing and filtering, we identified 1970 single cells with an average of 4,710 unique genes and 24,219 transcripts per cell (Figure S3A). Dimensionality reduction showed a clear separation between the two cell types (Figure S3B); two clusters one consisting exclusively of secretor cells and one of non-secretor cells were identified (Figure 2B). Differential gene expression analysis identified 322 genes were significantly enriched in the MDAMB231-S cells compared to MDAMB231-NS cells (adjusted $p < 0.05$; Table S1). We compared the differentially expressed genes (DEGs) to those previously associated with EV secretion.[29–31] Of the 322 DEGs we identified, 211 were annotated in the ExoCarta database as associated with EVs (Figure 2C, Table S2). When restricted to DEGs with greater than 1.2-fold difference between MDAMB231-S and MDAMB231-NS cells, we identified 34 genes known to be associated with EV secretion, metastasis, and invasion (Figures 2D and 2E, Table S3). We classified the DEGs into genes that encode cell-adhesion/migration-related proteins (*e.g.*, *ACTN1*, *CAV1*, *FXYD5*, and *DIAPH3*), transcriptional regulators (*e.g.*, *GTF3A*, *TFDP1*, and *SNAPC1*), and chaperones and heat shock proteins (*e.g.*, *HSP90AA1*, *HSPH1*, and *POMP*). Of these DEGs, *UBL3* encodes a protein that directly interacts

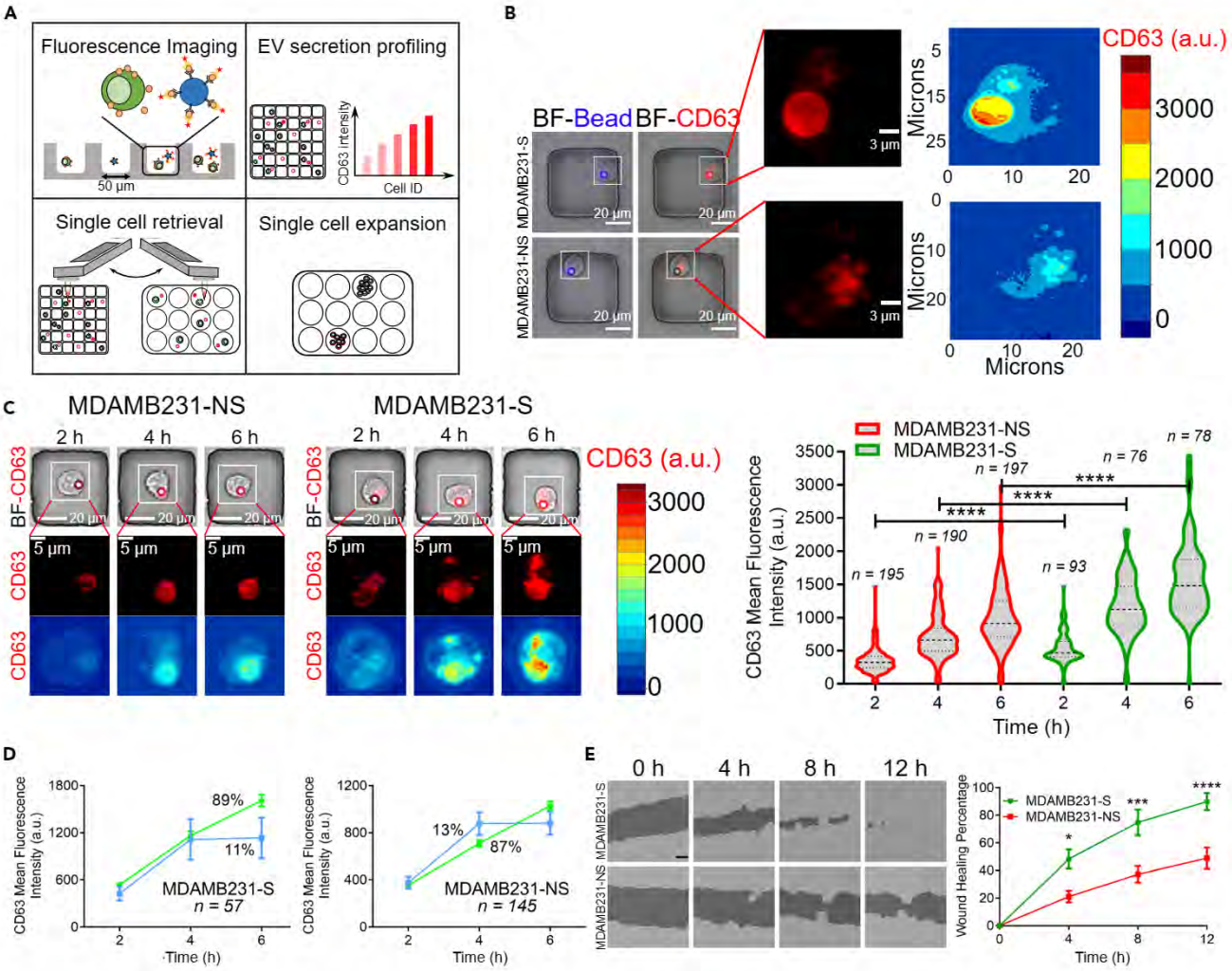

Figure 1. Establishment of monoclonal cell lines with different rates of EV secretion

(A) The workflow for the identification and isolation of single cells with differences in EV secretion capacity.

(B) Representative images of MDAMB231-S and MDAMB231-NS cells in wells (left), at high resolution (middle), and as contour maps of intensity of CD63.

(C) Images of (top to bottom) cells in wells, high resolution of CD63, and CD63 intensity contour maps of representative MDAMB231-NS (left) and MDAMB231-S (middle) cells at 2, 4, and 6 h. Right: Violin plots of medians and quantiles of CD63 intensities (****$p < 0.00001$; t-test).

(D) CD63 intensity as a function of time for MDAMB231-S (left) and MDAMB231-NS (right) cells plotted as means ± SEM. Two subpopulations are present: cells that continuously secrete EVs (green) and cells that secrete EVs in a burst at 2 h (blue).

(E) Left: Representative photographs of wound healing assays. Scale bar is 100 μm. Right: Plot of mean percent wound healed ±SEM versus time (n = 7 for each cell line; *$p < 0.05$, ***$p < 0.001$, and ****$p < 0.0001$; two-way ANOVA).

with CD63 and functions as a key post-translational modifier that facilitates the sorting of proteins into EVs.[32]

We posited that the genes associated with EV secretion or packaging within the EVs are regulated in a coordinated manner. Accordingly, we calculated the Spearman coefficient between the DEGs and applied a hierarchical clustering to identify the cluster of genes that were significantly correlated with each other. By applying a multiscale bootstrap resampling method, we identified that *HSP90AA1* was significantly correlated with *HSPH1*, *EIF5*, and *DIAPH3* (Figures 2F and 2G). We refer to these four genes as EV-sig genes. The transcripts of each of these four genes were significantly correlated with the levels of EV marker, *CD81* (Figure 2H). The proteins encoded by each of these genes have been individually shown to be associated with actin remodeling and EV secretion. *HSP90AA1* encodes HSP90, a molecular chaperone that promotes structural maintenance of proteins involved in cell cycle control and signal transduction. *HSPH1* encodes

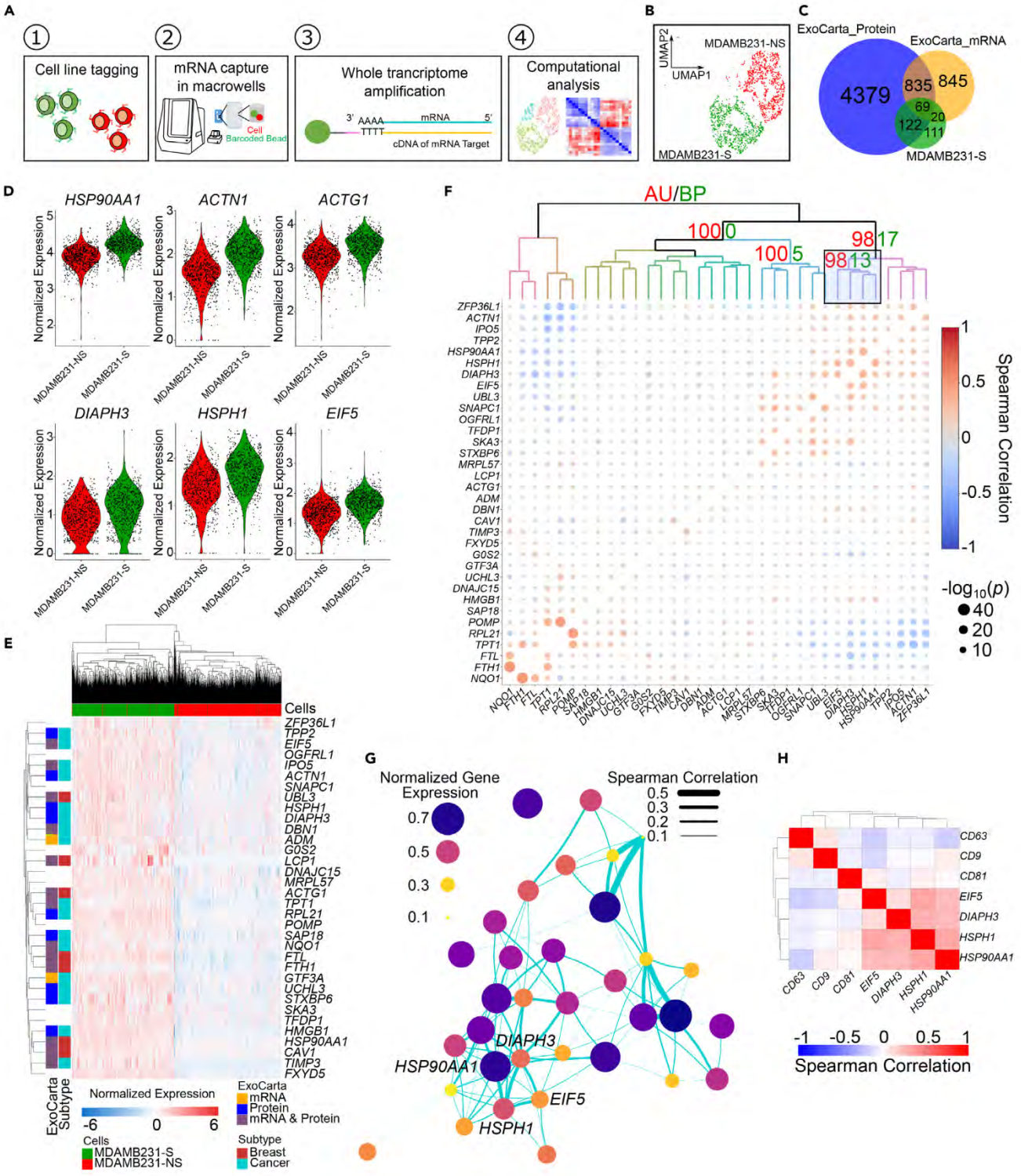

Figure 2. Identification of molecular signatures of EV secretion by scRNA-seq analysis

(A) The workflow of single-cell RNA-sequencing and whole transcriptome profiling for monoclonal cell lines.

(B) The UMAP plot of scRNA-seq data from MDAMB231-S and MDAMB231-NS cells.

(C) Venn diagram of the overlap of genes differentially expressed MDAMB231-S cells compared to MDAMB231-NS cells with mRNA and proteins from the ExoCarta dataset that are annotated as associated with EVs.

(D) Violin plots of genes upregulated in MDAMB231-S in comparison to MDAMB231-NS cells.

Figure 2. *Continued*

(E) Heatmap of the top 34 genes upregulated in MDAMB231-S cells. The colors to the left indicate ExoCarta annotation as associated with EV or linkage to breast cancer or other cancer types.

(F) Heatmap of Spearman coefficients for correlations between genes upregulated in MDAMB231-S cells relative to MDAMB231-NS cells. AU and BP indicate approximately unbiased and bootstrap probabilities, respectively. The correlations among EV-sig genes, *HSP90AA1, HSPH1, DIAPH3, and EIF5*, are highlighted.

(G) Network of top genes upregulated in MDAMB231-S cells relative to MDAMB231-NS cells with *HSP90AA1, HSPH1, DIAPH3, and EIF5* highlighted.

(H) Spearman correlation coefficients for four core EV genes and surface markers *CD63, CD81*, and *CD9* in MDAMB231-S cells.

a member of the heat shock protein 70 family of proteins that acts as a nucleotide exchange factor for molecular chaperones and is capable of direct protein-protein interaction with HSP90.[33] *DIAPH3* encodes a member of the diaphanous subfamily. DIAPH3 is involved in actin remodeling and regulation of the cell motility and adhesion and can activate the beta-catenin/T cell factor (TCF) signaling by binding to HSP90, which results in growth, migration, epithelial-mesenchymal transition, and metastasis in hepatocellular carcinoma cells.[34] *EIF5* encodes the eukaryotic translation initiation factor eIF5 that is enriched in EVs secreted from breast cancer cells and melanoma cells.[35]

To directly demonstrate a role for the EV-sig genes in EV secretion, we focused on HSP90 for three reasons: First, HSP90 interacts directly with both DIAPH3 and HSPH1.[33,34] Second, independent proteomic analyses of breast cancer cells showed that EVs contain both HSP90 and EIF5A.[32] Third, inhibitors of HSP90 are readily available, allowing us to study how inhibition of HSP90 impacts EV secretion from MDAMB231 cells. We used a standard transwell assay to capture the EVs secreted from MDAMB231 cells incubated with either tanespimycin (also known as 17AAG), a first generation HSP90 inhibitor, or ganetespib (also known as STA-9090), a potent, synthetic resorcinol-based HSP90 inhibitor (Figure S4A). The inhibition of HSP90 significantly reduced EV secretion in a dose-dependent manner even at nanomolar concentrations (Figure S4B). This observation further supports our hypothesis that EV-sig gene expression is a determinant of EV secretion.

EV-sig is predictive of EV secretion in breast cancer cell lines

To validate whether EV-sig can predict the secretion of EVs, we investigated three breast cancer cell lines, MDAMB231, MCF7, and HCC70, which have differences in metastatic potential. MDAMB231 and HCC70 cell lines were established from triple-negative breast cancers, whereas the MCF7 line is an estrogen receptor- and progesterone receptor-positive cancer cell line.[36] The wound healing assay confirmed that the migration potential of MDAMB231 cells is significantly higher than those of MCF7 and HCC70 cells (Figure 3A). We performed scRNA-seq on MDAMB231, MCF7, and HCC70 cells. We obtained an average of 4459 unique genes and 22,071 transcripts per cell (Figure S5A). After dimensionality reduction, the cells from each of the three cell lines clustered separately (Figure 3B), and a total of 2634 DEGs (> 1.2-fold change) were identified (Table S4).

To validate the phenotype of the cancer cell lines in the scRNA-seq data, we compared the expression of DEGs with known markers for breast cancer subtypes including luminal, basal A, and basal B.[36] This analysis showed that markers for luminal (e.g., *GATA3, FOXA1, KRT18*, and *KRT19*), basal A (e.g., *SLPI, KRT16*, and *KRT6B*), and basal B (e.g., *AXL, CAV1, VIM*, and *SEPRINE1*) subtype were upregulated in MCF7, HCC70, and MDAMB231 cells, respectively (Figure 3C). Similarly, pathway analysis confirmed that MDAMB231 and MCF7 cells are enriched for genes enriched in pathways corresponding to basal and luminal phenotypes, respectively (Figure 3D). Consistent with the fact that the HCC70 line was derived from a primary tumor, pathway analysis showed lower scores for metastatic and epithelial-mesenchymal transition pathways in HCC70 cells compared to the MDAMB231 and MCF7 cells (Figure 3E).

Next, we compared the average expression of EV-sig genes: HCC70 cells had the lowest expression, MCF7 cells had intermediate expression, and MDAMB231 cells had the highest expression (Figure 4A). Consistent with this observation, the Spearman correlation between the genes of the signature showed a significant correlation in the MDAMB231 cells; correlations were smaller in MCF7 and HCC70 cells (Figure 4B). At the protein level, we confirmed that all three cell lines expressed the HSP90 protein (Figure S5B). As an independent method to track the abundance of the EVs, we compared the levels of *CD63* and *CD81* mRNAs within the scRNA-seq data of these cell lines. All three lines expressed *CD63*; MDAMB231, and MCF7 cells expressed considerably higher levels of *CD81* mRNA than did HCC70 cells (Figures 4C and S5C).

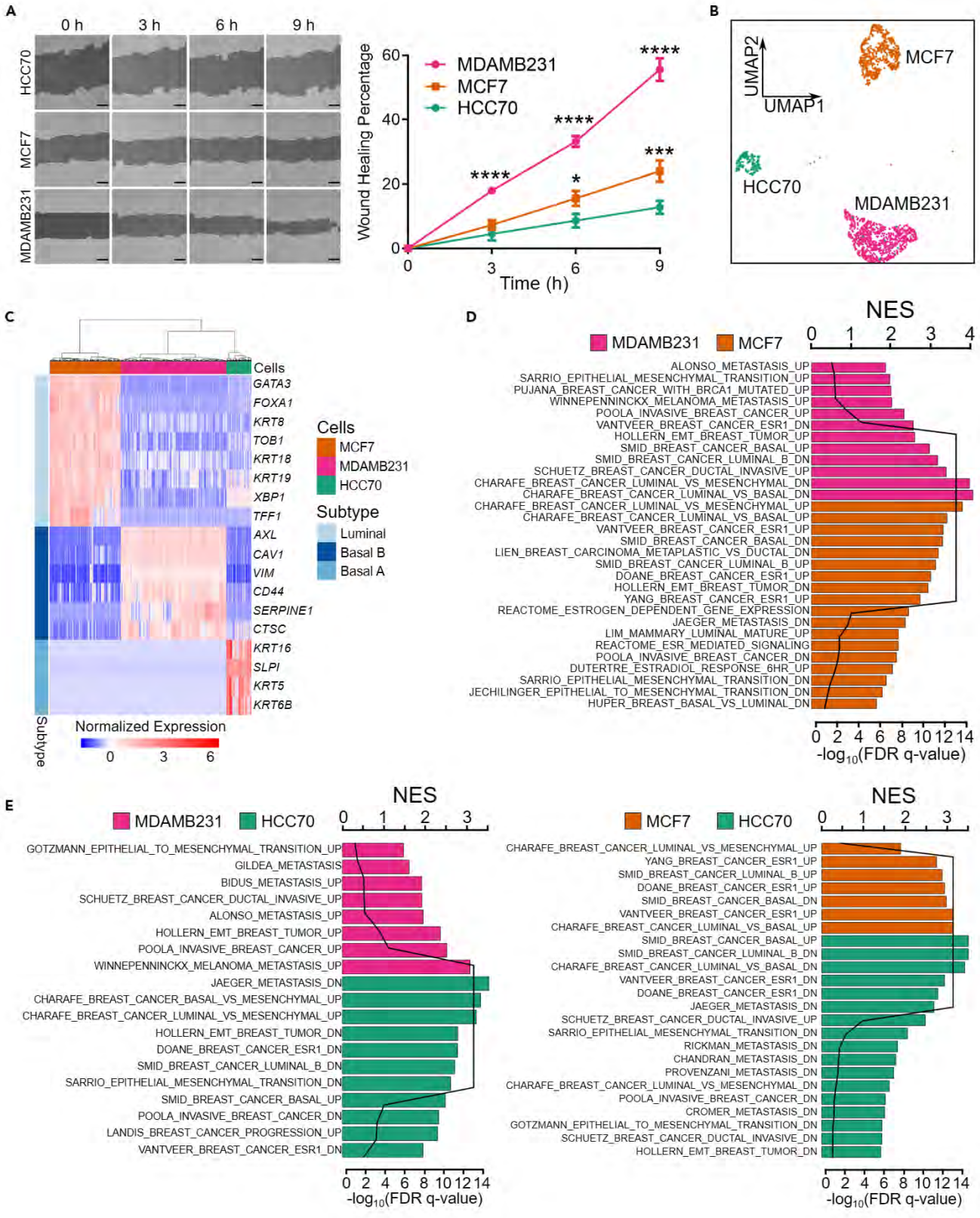
A
0 h
3 h
6 h
9 h
HCC70
MCF7
MDAMB231
Wound Healing Percentage
MDAMB231
MCF7
HCC70
Time (h)
B
UMAP2
UMAP1
MCF7
HCC70
MDAMB231
C
Cells
GATA3
FOXA1
KRT8
TOB1
KRT18
KRT19
XBP1
TFF1
AXL
CAV1
VIM
CD44
SERPINE1
CTSC
KRT16
SLPI
KRT5
KRT6B
Subtype
Normalized Expression
Luminal
Basal B
Basal A
D
NES
MDAMB231
MCF7
ALONSO_METASTASIS_UP
SARRIO_EPITHELIAL_MESENCHYMAL_TRANSITION_UP
PUJANA_BREAST_CANCER_WITH_BRCA1_MUTATED_UP
WINNEPENNINCKX_MELANOMA_METASTASIS_UP
POOLA_INVASIVE_BREAST_CANCER_UP
VANTVEER_BREAST_CANCER_ESR1_DN
HOLLERN_EMT_BREAST_TUMOR_UP
SMID_BREAST_CANCER_BASAL_UP
SMID_BREAST_CANCER_LUMINAL_B_DN
SCHUETZ_BREAST_CANCER_DUCTAL_INVASIVE_UP
CHARAFE_BREAST_CANCER_LUMINAL_VS_MESENCHYMAL_DN
CHARAFE_BREAST_CANCER_LUMINAL_VS_BASAL_DN
CHARAFE_BREAST_CANCER_LUMINAL_VS_MESENCHYMAL_UP
CHARAFE_BREAST_CANCER_LUMINAL_VS_BASAL_UP
VANTVEER_BREAST_CANCER_ESR1_UP
SMID_BREAST_CANCER_BASAL_DN
LIEN_BREAST_CARCINOMA_METAPLASTIC_VS_DUCTAL_DN
SMID_BREAST_CANCER_LUMINAL_B_UP
DOANE_BREAST_CANCER_ESR1_UP
HOLLERN_EMT_BREAST_TUMOR_DN
YANG_BREAST_CANCER_ESR1_UP
REACTOME_ESTROGEN_DEPENDENT_GENE_EXPRESSION
JAEGER_METASTASIS_DN
LIM_MAMMARY_LUMINAL_MATURE_UP
REACTOME_ESR_MEDIATED_SIGNALING
POOLA_INVASIVE_BREAST_CANCER_DN
DUTERTRE_ESTRADIOL_RESPONSE_6HR_UP
SARRIO_EPITHELIAL_MESENCHYMAL_TRANSITION_DN
JECHILINGER_EPITHELIAL_TO_MESENCHYMAL_TRANSITION_DN
HUPER_BREAST_BASAL_VS_LUMINAL_DN
-log10(FDR q-value)
E
NES
MDAMB231
HCC70
GOTZMANN_EPITHELIAL_TO_MESENCHYMAL_TRANSITION_UP
GILDEA_METASTASIS
BIDUS_METASTASIS_UP
SCHUETZ_BREAST_CANCER_DUCTAL_INVASIVE_UP
ALONSO_METASTASIS_UP
HOLLERN_EMT_BREAST_TUMOR_UP
POOLA_INVASIVE_BREAST_CANCER_UP
WINNEPENNINCKX_MELANOMA_METASTASIS_UP
JAEGER_METASTASIS_DN
CHARAFE_BREAST_CANCER_BASAL_VS_MESENCHYMAL_UP
CHARAFE_BREAST_CANCER_LUMINAL_VS_MESENCHYMAL_UP
HOLLERN_EMT_BREAST_TUMOR_DN
DOANE_BREAST_CANCER_ESR1_DN
SMID_BREAST_CANCER_LUMINAL_B_DN
SARRIO_EPITHELIAL_MESENCHYMAL_TRANSITION_DN
SMID_BREAST_CANCER_BASAL_UP
POOLA_INVASIVE_BREAST_CANCER_DN
LANDIS_BREAST_CANCER_PROGRESSION_UP
VANTVEER_BREAST_CANCER_ESR1_DN
-log10(FDR q-value)
NES
MCF7
HCC70
CHARAFE_BREAST_CANCER_LUMINAL_VS_MESENCHYMAL_UP
YANG_BREAST_CANCER_ESR1_UP
SMID_BREAST_CANCER_LUMINAL_B_UP
DOANE_BREAST_CANCER_ESR1_UP
SMID_BREAST_CANCER_BASAL_DN
VANTVEER_BREAST_CANCER_ESR1_UP
CHARAFE_BREAST_CANCER_LUMINAL_VS_BASAL_UP
SMID_BREAST_CANCER_BASAL_UP
SMID_BREAST_CANCER_LUMINAL_B_DN
CHARAFE_BREAST_CANCER_LUMINAL_VS_BASAL_DN
VANTVEER_BREAST_CANCER_ESR1_DN
DOANE_BREAST_CANCER_ESR1_DN
JAEGER_METASTASIS_DN
SCHUETZ_BREAST_CANCER_DUCTAL_INVASIVE_UP
SARRIO_EPITHELIAL_MESENCHYMAL_TRANSITION_DN
RICKMAN_METASTASIS_DN
CHANDRAN_METASTASIS_DN
PROVENZANI_METASTASIS_DN
CHARAFE_BREAST_CANCER_LUMINAL_VS_MESENCHYMAL_DN
POOLA_INVASIVE_BREAST_CANCER_DN
CROMER_METASTASIS_DN
GOTZMANN_EPITHELIAL_TO_MESENCHYMAL_TRANSITION_DN
SCHUETZ_BREAST_CANCER_DUCTAL_INVASIVE_DN
HOLLERN_EMT_BREAST_TUMOR_DN
-log10(FDR q-value)

Figure 3. EV secretion is correlated with migration in breast cancer cell lines

(A) Left: Representative images of wound healing assays showing the migration of MDAMB231, MCF7, and HCC70 cells over time. Scale bar is 100 μm. Right: Plot of mean percent wound healed ± SEM versus time (n = 9; *p < 0.05, ***p < 0.001, and ****p < 0.0001; two-way ANOVA).

(B) UMAP plot of scRNA-seq data from MDAMB231, MCF7, and HCC70 cells.

(C) Heatmap of expression of genes associated with luminal, basal A and basal B breast cancer subtypes in MDAMB231, MCF7, and HCC70 cell lines.

(D) Normalized enrichment scores (NESs) of pathways associated with metastatic cancer and luminal and basal breast cancer subtypes by pairwise comparison between MDAMB231 and MCF7 cells.

(E) NESs of pathways associated with metastatic cancer and luminal and basal breast cancer subtypes by pairwise comparisons between MDAMB231 and HCC70 cells (left) and between MCF7 and HCC70 cells (right).

We then utilized our single-cell assay to directly profile EV secretion from each of these three cell lines. As predicted by EV-sig, HCC70 cells secreted low amounts of EVs, MCF7 cells secreted intermediate levels, and MDAMB231 cells secreted high levels (Figure 4D). We also independently validated these results using the standard transwell assay (Figure S4A), and these results confirmed that HCC70 cells secreted fewer EVs than did MDAMB231 cells (Figures 4E and S6). We tracked the short-term kinetics of EV secretion, and at all the time points tested, individual MDAMB231 cells showed higher EV secretion than in single MCF7 cells (Figure 4F). Lastly, we tested the impact of HSP90 inhibitors demonstrating that both tanespimycin and ganetespib inhibited EV secretion from MCF7 cells (Figure S4). In summary, scRNA-seq and EV profiling results showed that more migratory cells secrete more EVs than less migratory cells and that EV-sig can predict the amount of EVs secreted by cells.

To generalize the value of EV-sig, we obtained gene expression data on 1,304 cell lines available in the Broad Institute Cancer Cell Line Encyclopedia (CCLE). Within this expanded dataset, expression of the EV-sig genes was highly correlated with each other (Figure S7A). Focusing specifically on breast cancer, EV-sig showed highest expression in basal B phenotypes, followed by basal A, then HER2-enriched, and then luminal (Figure S7B). This is consistent with the known aggressiveness of these subtypes of breast cancer.

EV-sig correlates with breast cancer outcomes

To investigate the translational value of EV-sig, we took advantage of the breast cancer datasets available in TCGA and METABRIC. We interrogated combined transcriptomic and clinical/pathological annotations for 1093 and 809 patients with breast cancer in TCGA and METABRIC, respectively. We first confirmed that the four genes that comprise EV-sig are significantly correlated with each other within human breast cancers (Figures 5A and S8A). We then stratified the patients into two groups: those with high EV-sig expression (BRCA_EV^{Hi} and MET_EV^{Hi}) and those with low EV-sig expression (BRCA_EV^{Lo} and MET_EV^{Lo}). The overall survival of patients with EV^{Hi} tumors was significantly lower than patients with EV^{Lo} tumors. For patients with data in TCGA, the median survival for patients with EV^{Hi} was 7.5 years, whereas those with EV^{Lo} the median survival was 10.8 years (HR: 2.3, 95% CI: 1.53–3.45); for patients with data in METABRIC, the median survival was 49.4 months for patients with EV^{Hi} and 63.6 months for EV^{Lo} (HR: 1.2, 95% CI: 1.03–1.40) (Figures 5B and S8B). Quantification of the pathology of the disease showed that EV-sig was associated with increased tumor size and more advanced disease (Figures 5C, 5D, and S8C).

We next evaluated whether EV-sig could be used to stratify the different molecular subtypes of breast cancers. The tumors with low levels of EV-sig expression were enriched in normal-like and luminal breast cancers, whereas tumors with high levels of EV-sig expression were enriched in basal breast cancers (Figures 5E and S8D). Gene set enrichment analysis (GSEA) specifically focused on pathways associated with tumor cell functions showed that tumors with high levels of EV-sig expression are enriched in pathways associated with invasiveness, metastasis, and epithelial to mesenchymal transition (Figures 5F and S8E). Taken together, the clinicopathological data are consistent with our *in vitro* observation that EV secretion is associated with increased aggressiveness and invasion of tumor cells.

To evaluate the nature and frequency of immune cell infiltration associated with higher expression of EV-sig genes; we quantified the relative frequencies of the 22 different immune cell types by evaluation of normalized gene expression data using the CIBERSORTx algorithm. Tumors classified as EV^{Lo} had an increased frequency of CD8$^+$ T cells increased cytolytic activity (associated with increased expression of both *PRF1* and *GZMA*), and increased frequency of *TBX21* expression in comparison to EV^{Hi} tumors (Figures 5G–5I and S8F). Collectively, these results suggest that increased EV secretion by cancer cells is associated with decreased CD8$^+$ T cell infiltration and that this in turn promotes growth of larger and more aggressive tumors.

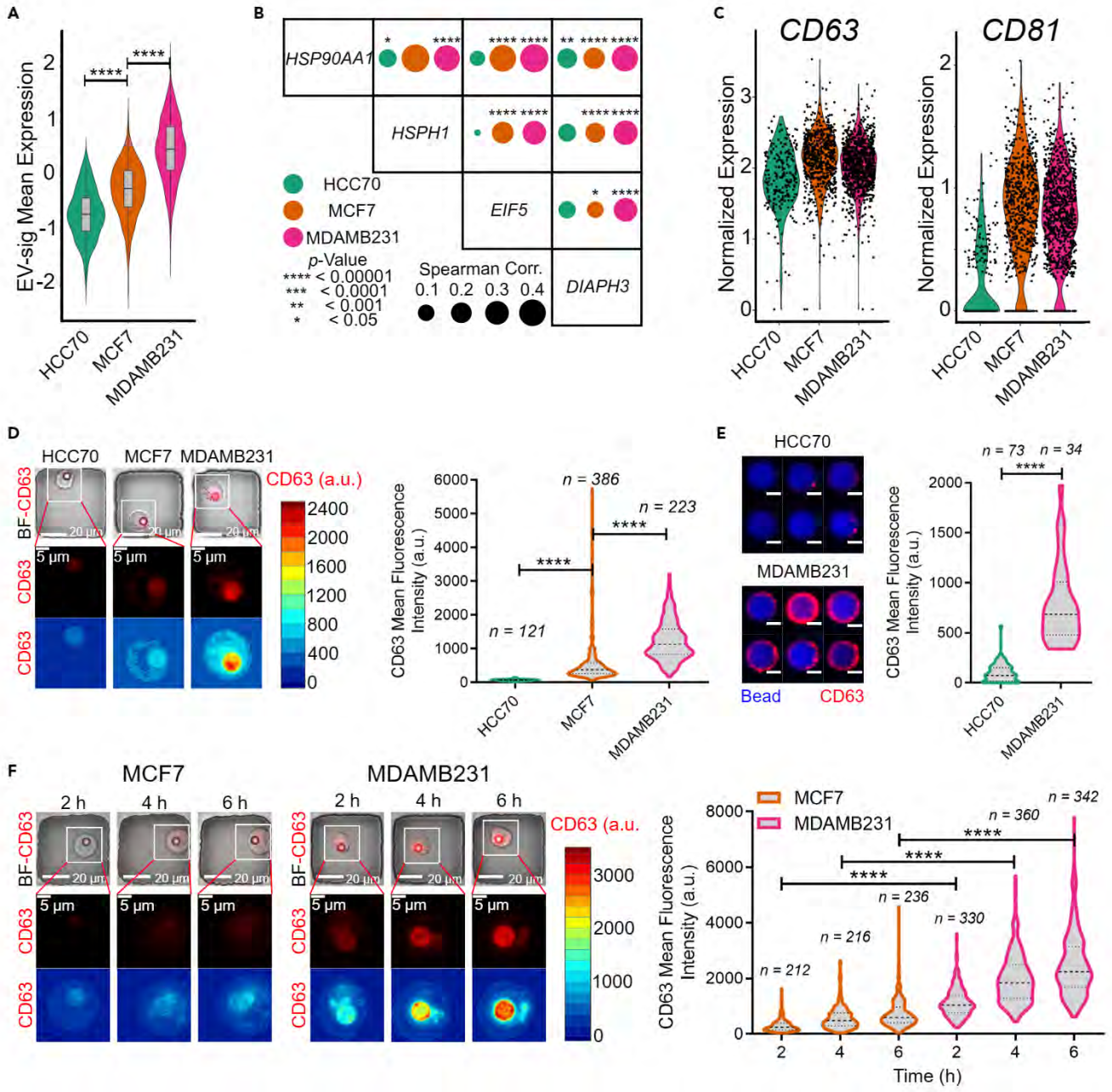

Figure 4. EV-sig is predictive of EV secretion from breast cancer cells

(A) Violin plots of average expression of EV-sig genes in MDAMB231, MCF7, and HCC70 cells (n = 227, 645, 971 for HCC70, MCF7, and HCC70 cells, respectively; ****p < 0.00001; t-test).

(B) Spearman correlation coefficients among EV-sig genes in MDAMB231, MCF7, and HCC70 cells.

(C) Violin plots showing the expression of *CD63* and *CD81* in MDAMB231, MCF7, and HCC70 cells.

(D) Left: Images of (top to bottom) cells in wells, high resolution of CD63 on cell, and CD63 intensity contour maps of representative MDAMB231, MCF7, and HCC70 cells at 6 h. Right: Violin plots of represent the median and quantiles of CD63 intensity (****p < 0.00001, t-test).

(E) Left: Images of representative functionalized beads in culture with MDAMB231 and HCC70 cell lines for 48 h in transwell assay. Scale bar is 3 µm. Right: Violin plots of the median and quantiles of CD63 intensities (****p < 0.0001; t-test).

(F) Images of (top to bottom) cells in wells, high resolution of CD63, and CD63 intensity contour maps of representative MCF7 cells (left) and MDAMB231 cells (Middle) at 2, 4, and 6 h. Right: Violin plots of the median and quantiles of CD63 intensities (****p < 0.00001; t-test).

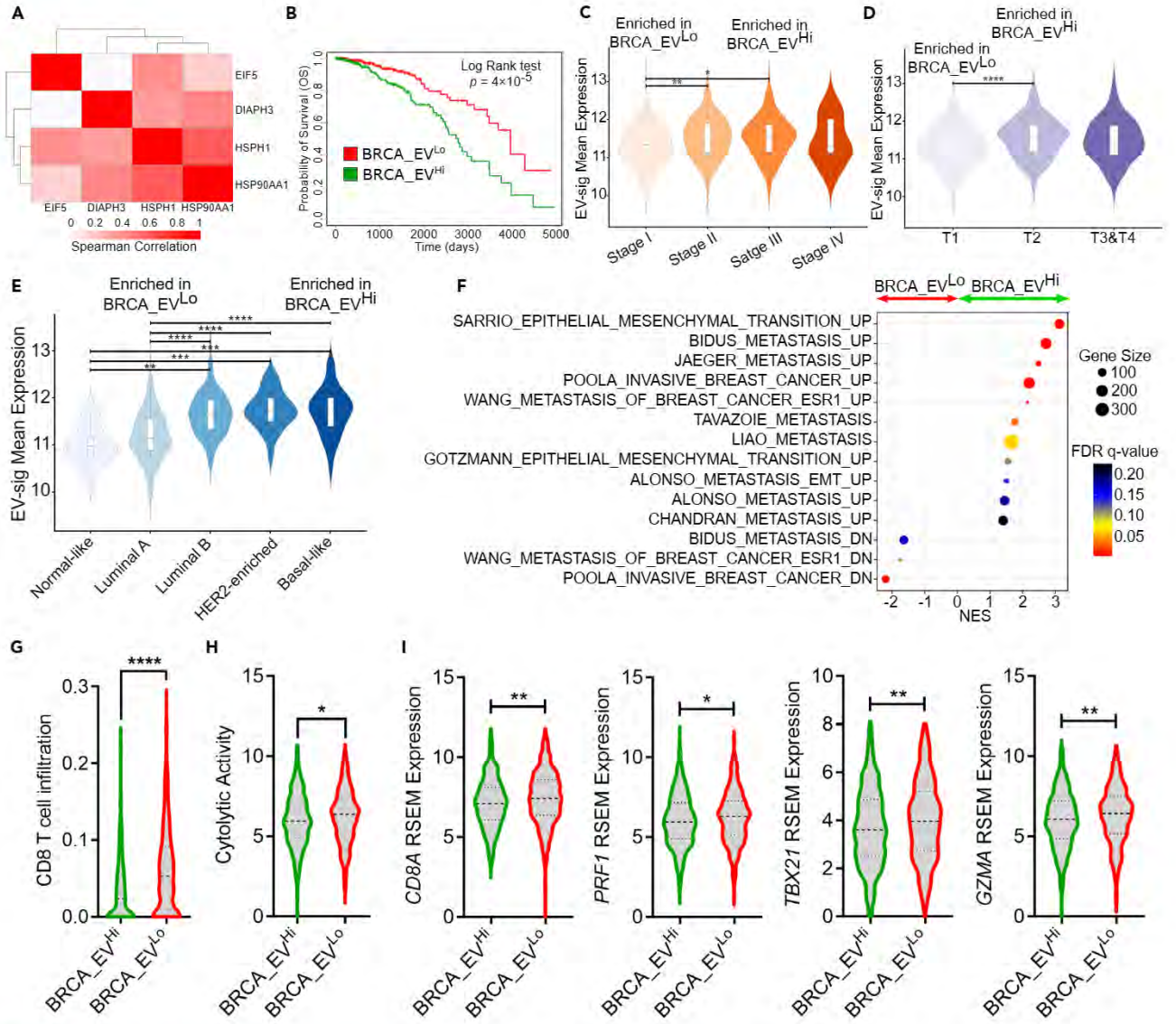

Figure 5. Expression of EV-sig genes is correlated with poor survival in breast cancer patients

(A) Spearman correlation coefficients of EV-sig genes in breast cancer patients from TCGA dataset.

(B) Overall survival of breast cancer patients divided by the median of the average expression of EV-sig genes (n = 547, and 546 for BRCA_EV^{Hi} and BRCA_EV^{Lo}, respectively).

(C) Violin plots of average expression of EV-sig genes by breast cancer stage (n = 108, 371, 153, and 13 for Stage I to V, respectively; *p < 0.05, **p < 0.01, ***p < 0.001, and ****p < 0.0001; one-way ANOVA).

(D) Violin plots of average expression of EV-sig genes by the size of the tumors with T1 the smallest (n = 174), T2 intermediate (n = 395), and T3 & T4 the largest (n = 94); (*p < 0.05, **p < 0.01, ***p < 0.001, and ****p < 0.0001; one-way ANOVA).

(E) Violin plots of average expression of EV-sig genes by the breast cancer subtype (n = 8, 191, 109, 53, and 83 for normal-like, luminal A, B, HER2-enriched, and basal-like subtypes, respectively; *p < 0.05, **p < 0.01, ***p < 0.001, and ****p < 0.0001; one-way ANOVA).

(F) NESs of pathways associated with metastasis in patients with high and low levels of EV-sig gene expression.

(G) CD8$^+$ T cells infiltration based on CIBERSORTx data for patients with high and low levels of EV-sig gene expression (****p < 0.0001; t-tests).

(H) Cytolytic activity scores and geometric means of *PRF1* and *GZMA* mRNA levels in patients with high and low levels of EV-sig gene expression (*p < 0.05; t-test).

(I) Normalized expression of CD8$^+$ T cell gene signature (*CD8A*, *PRF1*, *TBX21*, *GZMA*) in the patients with high and low levels of EV-sig gene expression (*p < 0.05, **p < 0.01, ***p < 0.001, and ****p < 0.0001; t-test).

To evaluate the value of EV-sig in the invasiveness of non-metastatic tumors, we obtained the gene expression of single cells from primary tumor tissues available on two datasets profiled by scRNA-seq. We evaluated 21 non-treated patients (GSE176078) compromised of 7 TNBC and 14 non-TNBC patients, and 5 patients (GSE180286) compromised of 2 TNBC and 3 non-TNBC patients (Figure S9A). Profiling the epithelial cells (EpCAM) (Figure S9B) showed distinct clusters (Figure S9C) compromised of TNBC and non-TNBC cancer cells (Figure S9D). We calculated the EV score using the AUCell method based on the expression of four EV-sig genes. The comparison between TNBC and non-TNBC patients showed a significant increase of EV score for the TNBC patients (Figure S9E). These results show that the expression of EV-sig genes is associated with increased aggressiveness in primary tumors.

DISCUSSION

EVs secreted by cancer cells have potential to serve as diagnostic markers, and EVs could be used for delivery of anticancer agents into tumors.[37–39] Techniques based on analysis of bulk cells have enabled classification of EVs, characterization of the cargoes of EVs, and investigation of the impact of EVs on the progression of tumors.[40] At the other end of the spectrum, single-vesicle profiling studies have revealed the heterogeneity of both surface markers and the internal cargo of EVs.[41–44] In the past few years, single-cell methods to map the heterogeneity in EV secretion across single cells have been developed.[45–47] We recently reported a method to profile secretion of EVs from single cancer cells using nanowell arrays[26] and here used this methodology to perform integrated profiling of the EV secretion and the transcriptional signature of EV-secreting cancer cells.

By profiling of populations of metastatic MDAMB231 breast cancer cells with differences in EV secretion, we identified several transcripts that are differentially expressed in cells that secrete EVs. These transcripts include proteins that were previously shown to play key roles in the biogenesis and secretion of EVs. As an example, *CAV1* encodes a protein that blocks the fusion of MVBs with autophagosomes.[48] EVs containing CAV1 have been shown to enhance the proliferation and invasion of metastatic cells.[49] Similarly, *UBL3* encodes a protein that was shown to enhance the sorting of cargo into EVs by functioning as a post-translational modification factor.[32] The majority of the proteins encoded by our DEGs were shown to interact UBL3 in MDAMB231 cells by unbiased proteomics, suggesting the importance of UBL3-mediated sorting of protein cargo into EVs.[32] Although initial studies suggested that the C-terminal CAAX motif, which is CVIL in UBL3, is important for membrane localization and substrate modification, how UBL3 identifies substrate proteins and mediates the transport of these proteins into EVs are not known.

Based on EV secretion analysis and scRNA-seq data from MDAMB231 cells, we derived a transcriptional signature of EV secretion, based on four genes, *HSP90AA1*, *HSPH1*, *EIF5*, and *DIAPH3*. The levels of these genes are strongly correlated with each other in cancer cell lines. We validated this signature by utilizing EV-sig to predict the EV secretion propensities of breast cancer cell lines and by inhibiting the activity of HSP90 *in vitro* and confirming that inhibition of HSP90 activity reduces EV secretion. We further demonstrated that expression of EV-sig genes is associated with aggressiveness of 1304 cell lines available in CCLE. The abundance of HSP90 in cancer EVs has been extensively documented, and it was recently shown that HSP90 is expressed in the EVs of more than 80% of cancer cell lines.[50] HSP90 is a pivotal regulator of proteostasis in cancer cells due to the high stress burden of these cells. In addition to its role as a chaperone, HSP90 also mediates the fusion of MVBs with the plasma membrane in yeast cells directly leading to secretion of EVs.[51] Somewhat surprisingly, tanespimycin, which traps HSP90 in the open conformation, was shown not to alter the membrane deformation (and presumably EV secretion) activity of *Drosophila* HSP90 expressed in yeast cells.[51] By contrast, our results directly evaluating EV secretion demonstrated that treatment of MDAMB231 cells with tanespimycin reduced EV secretion. The differences in these two results may be due to the differences in the readouts used to profile EV secretion: membrane deformation in the *Drosophila* cells vs. direct profiling of EV secretion here. The pivotal role for HSP90 in influencing secretion of EVs containing CD63 was independently confirmed via knockout of *HSP90*.[52]

To determine whether our EV-sig genes can act as biomarkers of EV secretion in patient biopsies, we investigated the correlation of EV-sig gene expression with outcome for patients whose data are available through The Cancer Genome Atlas (TCGA) and METABRIC databases. We discovered that elevated expression of EV-sig genes is associated with increased tumor size and stage of cancer and an enrichment

of more aggressive subtypes such as basal-like and HER2-enriched subtypes. Not surprisingly, elevated expression of EV-sig genes was associated with poor survival, and immune decomposition analyses revealed that tumors that express high levels of these genes were characterized by poor $CD8^+$ T cell infiltration.

In summary, we have performed integrated single-cell profiling of EV secretion and transcriptomes of breast cancer cells. We provided direct evidence for the role of HSP90 in EV secretion and showed that expression levels of four genes, which are correlated with EV secretion in cell lines, can be used to stratify tumor aggressiveness and survival within breast cancer patients. We anticipate the method, and the findings will have broad applications across cell types and diseases.

Limitation of the study

While our results identify the proteins correlated with EV secretion in breast cancer cells more mechanistic studies both *in vitro* and *in vivo* need to be undertaken to understand their individual/collective impact on EV secretion. We emphasize that while our results show a strong correlation between EV-sig genes and tumors with poor prognosis, we recognize that EV secretion is only one facet of tumor cell biology determining survival outcomes. Indeed even with the four genes, we have identified, they likely have multiple pleiotropic effects and we have studied EV secretion as the sole function. Nonetheless, our single-cell method represents a novel technique for directly linking EV secretion to molecular signatures at single-cell resolution and can facilitate the identification of proteins/pathways responsible for EV secretion.

STAR★METHODS

Detailed methods are provided in the online version of this paper and include the following:

- KEY RESOURCES TABLE
- RESOURCE AVAILABILITY
  - Lead contact
  - Material availability
  - Data and code availability
- EXPERIMENT MODEL AND SUBJECT DETAILS
  - Cell line
- METHOD DETAILS
  - Single-cell EV detection assay
  - Establishment of clonal cell lines
  - EV isolation and nanosight analysis
  - Wound healing assay
  - EV quantification using a transwell assay
  - Surface marker staining
  - Western blot methods
  - Single-cell RNA-sequencing
- QUANTIFICATION AND STATISTICAL ANALYSIS
  - Sequencing read alignments
  - Data processing and identification of differentially expressed genes
  - ExoCarta dataset analysis
  - Gene correlation analysis
  - Gene set enrichment analysis for breast cancer cell lines
  - Core signature identification and network analysis
  - Cancer cell line encyclopedia (CCLE) analysis
  - TCGA and METABRIC analyses
  - scRNA-seq analysis of primary tumors

SUPPLEMENTAL INFORMATION

Supplemental information can be found online at https://doi.org/10.1016/j.isci.2023.106482.

ACKNOWLEDGMENTS

This work was supported in part by the NIH (R01GM143243) and CPRIT (RP180466), to N.V. and by the Cancer Prevention Research Institute of Texas (CPRIT) Multi-Investigator Research Award (RP160710) to S.A.M.

AUTHOR CONTRIBUTIONS

N.V. and M.F. designed the study. M.F. performed *in vitro* study. M.M.*P. and* A.R. performed scRNA-seq. M.F. performed scRNA-seq analysis. M.F. and V.K. performed TCGA and METABRIC analysis. M.J.M. performed western blotting and EV isolation. K.C., S.A.M., and N.V. supervised the study.

DECLARATION OF INTERESTS

UH has filed a provisional patent based on some of the technologies described in this manuscript.

INCLUSION AND DIVERSITY

One or more of the authors of this paper self-identifies as an underrepresented ethnic minority in their field of research or within their geographical location.

Received: September 2, 2022
Revised: February 2, 2023
Accepted: March 10, 2023
Published: March 21, 2023

REFERENCES

1. Valadi, H., Ekström, K., Bossios, A., Sjöstrand, M., Lee, J.J., and Lötvall, J.O. (2007). Exosome-mediated transfer of mRNAs and microRNAs is a novel mechanism of genetic exchange between cells. Nat. Cell Biol. *9*, 654–659. https://doi.org/10.1038/ncb1596.

2. Balaj, L., Lessard, R., Dai, L., Cho, Y.J., Pomeroy, S.L., Breakefield, X.O., and Skog, J. (2011). Tumour microvesicles contain retrotransposon elements and amplified oncogene sequences. Nat. Commun. *2*, 180. https://doi.org/10.1038/ncomms1180.

3. Kahlert, C., and Kalluri, R. (2013). Exosomes in tumor microenvironment influence cancer progression and metastasis. J. Mol. Med. *91*, 431–437. https://doi.org/10.1007/s00109-013-1020-6.

4. Raposo, G., and Stoorvogel, W. (2013). Extracellular vesicles: exosomes, microvesicles, and friends. J. Cell Biol. *200*, 373–383. https://doi.org/10.1083/jcb.201211138.

5. Théry, C., Zitvogel, L., and Amigorena, S. (2002). Exosomes: composition, biogenesis and function. Nat. Rev. Immunol. *2*, 569–579. https://doi.org/10.1038/nri855.

6. Dickhout, A., and Koenen, R.R. (2018). Extracellular vesicles as biomarkers in cardiovascular disease; chances and risks. Front. Cardiovasc. Med. *5*, 113. https://doi.org/10.3389/fcvm.2018.00113.

7. Nazarenko, I., Rana, S., Baumann, A., McAlear, J., Hellwig, A., Trendelenburg, M., Lochnit, G., Preissner, K.T., and Zöller, M. (2010). Cell surface tetraspanin Tspan8 contributes to molecular pathways of exosome-induced endothelial cell activation. Cancer Res. *70*, 1668–1678. https://doi.org/10.1158/0008-5472.CAN-09-2470.

8. Yang, Y., Li, C.W., Chan, L.C., Wei, Y., Hsu, J.M., Xia, W., Cha, J.H., Hou, J., Hsu, J.L., Sun, L., and Hung, M.C. (2018). Exosomal PD-L1 harbors active defense function to suppress T cell killing of breast cancer cells and promote tumor growth. Cell Res. *28*, 862–864. https://doi.org/10.1038/s41422-018-0060-4.

9. Hendrix, A., Maynard, D., Pauwels, P., Braems, G., Denys, H., Van den Broecke, R., Lambert, J., Van Belle, S., Cocquyt, V., Gespach, C., et al. (2010). Effect of the secretory small GTPase Rab27B on breast cancer growth, invasion, and metastasis. J. Natl. Cancer Inst. *102*, 866–880. https://doi.org/10.1093/jnci/djq153.

10. Rana, S., Malinowska, K., and Zöller, M. (2013). Exosomal tumor microRNA modulates premetastatic organ cells. Neoplasia *15*, 281–295. https://doi.org/10.1593/neo.122010.

11. Jiang, C., Fu, Y., Liu, G., Shu, B., Davis, J., and Tofaris, G.K. (2021). Multiplexed profiling of extracellular vesicles for biomarker development. Nano-Micro Lett. *14*, 3. https://doi.org/10.1007/S40820-021-00753-W.

12. Fraser, K., Jo, A., Giedt, J., Vinegoni, C., Yang, K.S., Peruzzi, P., Chiocca, E.A., Breakefield, X.O., Lee, H., and Weissleder, R. (2019). Characterization of single microvesicles in plasma from glioblastoma patients. Neuro Oncol. *21*, 606–615. https://doi.org/10.1093/NEUONC/NOY187.

13. Wang, S.U., Khan, A., Huang, R., Ye, S., Di, K., Xiong, T., and Li, Z. (2020). Recent advances in single extracellular vesicle detection methods. Biosens. Bioelectron. *154*, 112056. https://doi.org/10.1016/J.BIOS.2020.112056.

14. Teng, F., and Fussenegger, M. (2020). Shedding light on extracellular vesicle biogenesis and bioengineering. Adv. Sci. *8*, 2003505. https://doi.org/10.1002/ADVS.202003505.

15. Katzmann, D.J., Babst, M., and Emr, S.D. (2001). Ubiquitin-dependent sorting into the multivesicular body pathway requires the function of a conserved endosomal protein sorting complex, ESCRT-I. Cell *106*, 145–155. https://doi.org/10.1016/S0092-8674(01)00434-2.

16. Henne, W.M., Stenmark, H., and Emr, S.D. (2013). Molecular mechanisms of the membrane sculpting ESCRT pathway. Cold Spring Harb. Perspect. Biol. *5*, a016766. https://doi.org/10.1101/cshperspect.a016766.

17. Trajkovic, K., Hsu, C., Chiantia, S., Rajendran, L., Wenzel, D., Wieland, F., Schwille, P., Brügger, B., and Simons, M. (2008). Ceramide triggers budding of exosome vesicles into multivesicular endosomes. Science *319*, 1244–1247. https://doi.org/10.1126/science.1153124.

18. Van Niel, G., Charrin, S., Simoes, S., Romao, M., Rochin, L., Saftig, P., Marks, M.S., Rubinstein, E., and Raposo, G. (2011). The tetraspanin CD63 regulates ESCRT-independent and-dependent endosomal sorting during melanogenesis. Dev. Cell *21*, 708–721. https://doi.org/10.1016/j.devcel.2011.08.019.

19. Fader, C.M., Sánchez, D.G., Mestre, M.B., and Colombo, M.I. (2009). TI-VAMP/VAMP7 and VAMP3/cellubrevin: two v-SNARE proteins involved in specific steps of the autophagy/multivesicular body pathways. Biochim. Biophys. Acta *1793*, 1901–1916. https://doi.org/10.1016/j.bbamcr.2009.09.011.

20. Zylbersztejn, K., and Galli, T. (2011). Vesicular traffic in cell navigation. FEBS J. *278*, 4497–4505. https://doi.org/10.1111/j.1742-4658.2011.08168.x.

21. Ostrowski, M., Carmo, N.B., Krumeich, S., Fanget, I., Raposo, G., Savina, A., Moita, C.F., Schauer, K., Hume, A.N., Freitas, R.P., et al. (2010). Rab27a and Rab27b control different steps of the exosome secretion pathway. Nat. Cell Biol. *12*, 19–30. https://doi.org/10.1038/ncb2000.

22. Baietti, M.F., Zhang, Z., Mortier, E., Melchior, A., Degeest, G., Geeraerts, A., Ivarsson, Y., Depoortere, F., Coomans, C., Vermeiren, E., et al. (2012). Syndecan–syntenin–ALIX regulates the biogenesis of exosomes. Nat. Cell Biol. *14*, 677–685. https://doi.org/10.1038/ncb2502.

23. Kalluri, R. (2016). The biology and function of exosomes in cancer. J. Clin. Invest. *126*, 1208–1215. https://doi.org/10.1172/JCI81135.

24. Hessvik, N.P., and Llorente, A. (2018). Current knowledge on exosome biogenesis and release. Cell. Mol. Life Sci. *75*, 193–208. https://doi.org/10.1007/s00018-017-2595-9.

25. Yang, S.S., Ma, S., Dou, H., Liu, F., Zhang, S.Y., Jiang, C., Xiao, M., and Huang, Y.X. (2020). Breast cancer-derived exosomes regulate cell invasion and metastasis in breast cancer via miR-146a to activate cancer associated fibroblasts in tumor microenvironment. Exp. Cell Res. *391*, 111983. https://doi.org/10.1016/j.yexcr.2020.111983.

26. Fathi, M., Joseph, R., Adolacion, J.R.T., Martinez-Paniagua, M., An, X., Gabrusiewicz, K., Mani, S.A., and Varadarajan, N. (2021). Single-cell cloning of breast cancer cells secreting specific subsets of extracellular vesicles. Cancers *13*, 4397. https://doi.org/10.3390/CANCERS13174397.

27. Risha, Y., Minic, Z., Ghobadloo, S.M., and Berezovski, M.V. (2020). The proteomic analysis of breast cell line exosomes reveals disease patterns and potential biomarkers. Sci. Rep. *10*, 13572. https://doi.org/10.1038/s41598-020-70393-4.

28. Zhang, N., Zuo, L., Zheng, H., Li, G., and Hu, X. (2018). Increased expression of CD81 in breast cancer tissue is associated with reduced patient prognosis and increased cell migration and proliferation in MDA-MB-231 and MDA-MB-435S human breast cancer cell lines in vitro. Med. Sci. Monit. *24*, 5739–5747. https://doi.org/10.12659/MSM.911612.

29. Keerthikumar, S., Chisanga, D., Ariyaratne, D., Al Saffar, H., Anand, S., Zhao, K., Samuel, M., Pathan, M., Jois, M., Chilamkurti, N., et al. (2016). ExoCarta: a web-based compendium of exosomal cargo. J. Mol. Biol. *428*, 688–692. https://doi.org/10.1016/j.jmb.2015.09.019.

30. Mathivanan, S., Fahner, C.J., Reid, G.E., and Simpson, R.J. (2012). ExoCarta 2012: database of exosomal proteins, RNA and lipids. Nucleic Acids Res. *40*, D1241–D1244. https://doi.org/10.1093/nar/gkr828.

31. Mathivanan, S., and Simpson, R.J. (2009). ExoCarta: a compendium of exosomal proteins and RNA. Proteomics *9*, 4997–5000. https://doi.org/10.1002/pmic.200900351.

32. Ageta, H., Ageta-Ishihara, N., Hitachi, K., Karayel, O., Onouchi, T., Yamaguchi, H., Kahyo, T., Hatanaka, K., Ikegami, K., Yoshioka, Y., et al. (2018). UBL3 modification influences protein sorting to small extracellular vesicles. Nat. Commun. *9*, 3936. https://doi.org/10.1038/S41467-018-06197-Y.

33. Fan, G., Tu, Y., Wu, N., and Xiao, H. (2020). The expression profiles and prognostic values of HSPs family members in Head and neck cancer. Cancer Cell Int. *20*, 220. https://doi.org/10.1186/s12935-020-01296-7.

34. Dong, L., Li, Z., Xue, L., Li, G., Zhang, C., Cai, Z., Li, H., and Guo, R. (2018). DIAPH3 promoted the growth, migration and metastasis of hepatocellular carcinoma cells by activating beta-catenin/TCF signaling. Mol. Cell. Biochem. *438*, 183–190. https://doi.org/10.1007/s11010-017-3125-7.

35. Gangoda, L., Liem, M., Ang, C., Keerthikumar, S., Adda, C.G., Parker, B.S., and Mathivanan, S. (2017). Proteomic profiling of exosomes secreted by breast cancer cells with varying metastatic potential. Proteomics *17*, 1600370. https://doi.org/10.1002/PMIC.201600370.

36. Dai, X., Cheng, H., Bai, Z., and Li, J. (2017). Breast cancer cell line classification and its relevance with breast tumor subtyping. J. Cancer *8*, 3131–3141. https://doi.org/10.7150/jca.18457.

37. Cheng, S., Li, Y., Yan, H., Wen, Y., Zhou, X., Friedman, L., and Zeng, Y. (2021). Advances in microfluidic extracellular vesicle analysis for cancer diagnostics. Lab Chip *21*, 3219–3243. https://doi.org/10.1039/D1LC00443C.

38. Jabbari, N., Akbariazar, E., Feqhhi, M., Rahbarghazi, R., and Rezaie, J. (2020). Breast cancer-derived exosomes: tumor progression and therapeutic agents. J. Cell. Physiol. *235*, 6345–6356. https://doi.org/10.1002/JCP.29668.

39. Jiang, L., Gu, Y., Du, Y., and Liu, J. (2019). Exosomes: diagnostic biomarkers and therapeutic delivery vehicles for cancer. Mol. Pharm. *16*, 3333–3349. https://doi.org/10.1021/acs.molpharmaceut.9b00409.

40. Xu, R., Greening, D.W., Zhu, H.J., Takahashi, N., and Simpson, R.J. (2016). Extracellular vesicle isolation and characterization: toward clinical application. J. Clin. Invest. *126*, 1152–1162. https://doi.org/10.1172/JCI81129.

41. Lee, K., Fraser, K., Ghaddar, B., Yang, K., Kim, E., Balaj, L., Chiocca, E.A., Breakefield, X.O., Lee, H., and Weissleder, R. (2018). Multiplexed profiling of single extracellular vesicles. ACS Nano *12*, 494–503. https://doi.org/10.1021/acsnano.7b07060.

42. Chiu, Y.J., Cai, W., Shih, Y.R.V., Lian, I., and Lo, Y.H. (2016). A single-cell assay for time lapse studies of exosome secretion and cell behaviors. Small *12*, 3658–3666. https://doi.org/10.1002/smll.201600725.

43. Son, K.J., Rahimian, A., Shin, D.S., Siltanen, C., Patel, T., and Revzin, A. (2016). Microfluidic compartments with sensing microbeads for dynamic monitoring of cytokine and exosome release from single cells. Analyst *141*, 679–688. https://doi.org/10.1039/c5an01648g.

44. Verweij, F.J., Bebelman, M.P., Jimenez, C.R., Garcia-Vallejo, J.J., Janssen, H., Neefjes, J., Knol, J.C., de Goeij-de Haas, R., Piersma, S.R., Baglio, S.R., et al. (2018). Quantifying exosome secretion from single cells reveals a modulatory role for GPCR signaling. J. Cell Biol. *217*, 1129–1142. https://doi.org/10.1083/jcb.201703206.

45. Ji, Y., Qi, D., Li, L., Su, H., Li, X., Luo, Y., Sun, B., Zhang, F., Lin, B., Liu, T., and Lu, Y. (2019). Multiplexed profiling of single-cell extracellular vesicles secretion. Proc. Natl. Acad. Sci. USA *116*, 5979–5984. https://doi.org/10.1073/pnas.1814348116.

46. Ko, J., Wang, Y., Sheng, K., Weitz, D.A., and Weissleder, R. (2021). Sequencing-based protein analysis of single extracellular vesicles. ACS Nano *15*, 5631–5638. https://doi.org/10.1021/acsnano.1c00782.

47. Wu, D., Yan, J., Shen, X., Sun, Y., Thulin, M., Cai, Y., Wik, L., Shen, Q., Oelrich, J., Qian, X., et al. (2019). Profiling surface proteins on individual exosomes using a proximity barcoding assay. Nat. Commun. *10*, 3854. https://doi.org/10.1038/s41467-019-11486-1.

48. Dias, M.V.S., Teixeira, B.L., Rodrigues, B.R., Sinigaglia-Coimbra, R., Porto-Carreiro, I., Roffé, M., Hajj, G.N.M., and Martins, V.R. (2016). PRNP/prion protein regulates the secretion of exosomes modulating CAV1/caveolin-1-suppressed autophagy. Autophagy *12*, 2113–2128. https://doi.org/10.1080/15548627.2016.1226735.

49. Campos, A., Burgos-Ravanal, R., González, M.F., Huilcaman, R., Lobos González, L., and Quest, A.F.G. (2019). Cell intrinsic and extrinsic mechanisms of caveolin-1-enhanced metastasis. Biomolecules *9*, 314. https://doi.org/10.3390/biom9080314.

50. Hoshino, A., Kim, H.S., Bojmar, L., Gyan, K.E., Cioffi, M., Hernandez, J., Zambirinis, C.P., Rodrigues, G., Molina, H., Heissel, S., et al. (2020). Extracellular vesicle and particle biomarkers define multiple human cancers. Cell *182*, 1044–1061.e18. https://doi.org/10.1016/j.cell.2020.07.009.

51. Lauwers, E., Wang, Y.C., Gallardo, R., Van der Kant, R., Michiels, E., Swerts, J., Baatsen, P., Zaiter, S.S., McAlpine, S.R., Gounko, N.V., et al. (2018). Hsp90 mediates membrane deformation and exosome release. Mol. Cell *71*, 689–702.e9. https://doi.org/10.1016/J.MOLCEL.2018.07.016.

52. Tang, X., Chang, C., Guo, J., Lincoln, V., Liang, C., Chen, M., Woodley, D.T., and Li, W. (2019). Tumour-secreted Hsp90α on external surface of exosomes mediates tumour-stromal cell communication via autocrine and paracrine mechanisms. Sci. Rep. *9*, 15108. https://doi.org/10.1038/s41598-019-51704-w.

53. Gebäck, T., Schulz, M.M.P., Koumoutsakos, P., and Detmar, M. (2009). TScratch: a novel and simple software tool for automated analysis of monolayer wound healing assays: short Technical Reports. Biotechniques *46*, 265–274. https://doi.org/10.2144/000113083.

54. Stuart, T., Butler, A., Hoffman, P., Hafemeister, C., Papalexi, E., Mauck, W.M., 3rd, Hao, Y., Stoeckius, M., Smibert, P., and Satija, R. (2019). Comprehensive integration of single-cell data. Cell *177*, 1888–1902.e21. https://doi.org/10.1016/j.cell.2019.05.031.

55. Suzuki, R., and Shimodaira, H. (2006). Pvclust: an R package for assessing the uncertainty in hierarchical clustering. Bioinformatics *22*, 1540–1542. https://doi.org/10.1093/bioinformatics/btl117.

56. Csardi, G., and Nepusz, T. (2006). The igraph software package for complex network research. InterJournal Complex Syst *1695*, 1–9. https://igraph.org.

57. Love, M.I., Huber, W., and Anders, S. (2014). Moderated estimation of fold change and dispersion for RNA-seq data with DESeq2. Genome Biol. *15*, 550. https://doi.org/10.1186/s13059-014-0550-8.

58. Rooney, M.S., Shukla, S.A., Wu, C.J., Getz, G., and Hacohen, N. (2015). Molecular and genetic properties of tumors associated with local immune cytolytic activity. Cell *160*, 48–61. https://doi.org/10.1016/j.cell.2014.12.033.

59. Wu, S.Z., Al-Eryani, G., Roden, D.L., Junankar, S., Harvey, K., Andersson, A., Thennavan, A., Wang, C., Torpy, J.R., Bartonicek, N., et al. (2021). A single-cell and spatially resolved atlas of human breast cancers. Nat. Genet. *53*, 1334–1347. https://doi.org/10.1038/s41588-021-00911-1.

60. Xu, K., Wang, R., Xie, H., Hu, L., Wang, C., Xu, J., Zhu, C., Liu, Y., Gao, F., Li, X., et al. (2021). Single-cell RNA sequencing reveals cell heterogeneity and transcriptome profile of breast cancer lymph node metastasis. Oncogenesis *10*, 66. https://doi.org/10.1038/s41389-021-00355-6.

61. Aibar, S., González-Blas, C.B., Moerman, T., Huynh-Thu, V.A., Imrichova, H., Hulselmans, G., Rambow, F., Marine, J.C., Geurts, P., Aerts, J., et al. (2017). SCENIC: single-cell regulatory network inference and clustering. Nat. Methods *14*, 1083–1086. https://doi.org/10.1038/nmeth.4463.

STAR★METHODS

KEY RESOURCES TABLE

REAGENT or RESOURCE	SOURCE	IDENTIFIER
Antibodies		
biotin anti-CD81 antibody	Biolegend	Cat#349514; RRID:AB_2572038
PE anti-CD63 antibody	Biolegend	Cat#353003; RRID:AB_10896786
rabbit anti-HSP90alpha antibody	Cell Signaling Technology	Cat#8165S; RRID:AB_11217436
anti-rabbit IgG HRP-conjugated antibody	Jackson ImmunoResearch	Cat#111-035-144; RRID:AB_2307391
anti-β-actin antibody	Biolegend	Cat#643802; RRID:AB_2223199
anti-mouse IgG HRP-linked antibody	Cell Signaling Technology	Cat#7076S; RRID:AB_330924
Chemicals, peptides, and recombinant proteins		
PE Streptavidin	Biolegend	Cat#405203
PLL-g-PEG	SuSoS	PLL(20)-g[3.5]- PEG(2)
Tanespimycin	medchemexpress	Cat#HY-10211
ganetespib	medchemexpress	Cat#HY-15205
RIPA buffer	Millipore Sigma	Cat#20-188
protease inhibitor cocktail	ThermoScientific	Cat#1862209
4x Laemmli sample buffer	BioRad	Cat#1610747
2-mercaptoethanol	Sigma Life Science	Cat#M3148-20ML
polyacrylamide gel	BioRad	Cat#4561084
bovine serum albumin (BSA)	Fisher Bioreagents	Cat#BP1600-100
Pierce 1-Step Ultra TMB Blotting Solution	ThermoScientific	Cat#37574
Fetal Bovine Serum (FBS)	R&D Systems	Cat#S11150
RPMI 1640 W/GLN	Corning	Cat#10040CV
EME W/GLN	Quality Biological	Cat#112018101
Penicillin : Streptomycin	Corning	Cat#30-002-CI
HEPES	Cytiva	Cat#SH30237.01
MEM Non-Essential Amino Acids	Corning	Cat#25025CI
L-Glutamine	Corning	Cat#25-005-CI
1x tris	J.T Baker	Cat#4109-02
glycine	Sigma Life Science	Cat#56-40-6
SDS	Hoefer	Cat#151-21-3
Methanol	BDH Chemicals	Cat#67-56-1
Polyvinylidene Fluoride (PVDF) membrane	Amersham Hybond	Cat#10600023
TWEEN20	SIGMA	Cat#P7949-500ML
Critical commercial assays		
BD Human Immune Single-Cell Multiplexing Kit	BD Biosciences	Cat#633781
BD Rhapsody™ Whole Transcriptome Analysis (WTA) Amplification Kit	BD Biosciences	Cat#633802
Pierce BCA Assay Kit	Thermofisher	Cat#23227
PKH67	Sigma-Aldrich	Cat#PKH67GL-1KT
LumAvidin beads	Luminex	Cat#L100-L115-01
ExoQuick-TC	System Biosciences	Cat#EQULTRA-20TC-1

(*Continued on next page*)

Continued

REAGENT or RESOURCE	SOURCE	IDENTIFIER
Deposited data		
ExoCarta	ExoCarta	http://exocarta.org/download.
Cancer Cell Line Encyclopedia (CCLE)	Broad Institute	DepMap portal (https://depmap.org/portal/download/)
The Cancer Genome Atlas	National Cancer Institute (NCI) and National Human Genome Research Institute (NHGRI)	Broad Institute FireBrowse Data Portal (www.firebrowse.org)
The Molecular Taxonomy of Breast Cancer International Consortium (METABRIC)	Cambridge Research Institute and British Columbia Cancer Centre	cbioportal for cancer genome (www.cbioportal.org)
GEO single-cell RNA-seq	This study	GSE211561
GEO single-cell RNA-seq	GSE180286	GSE180286
GEO single-cell RNA-seq	GSE176078	GSE176078
Experimental models: Cell lines		
MDA-MB-231	ATCC	HTB-26
MCF7	ATCC	HTB-22
HCC70	ATCC	CRL-2315
Software and algorithms		
BD Rhapsody™ WTA Analysis Pipeline	Seven Bridges	https://igor.sbgenomics.com/public/apps/#jiewho/bd-public-project/bd-rhapsody-wta-analysis-pipeline/
Seurat (v 3.0)	Satija lab	https://satijalab.org/seurat/
GraphPad Prism	GraphPad	V9.0
R (v 4.0.1)	R	R: The R Project for Statistical Computing (r-project.org)
GSEA	UC San Diego and Broad Institute	GSEA (gsea-msigdb.org)
CIBERSORTx	CIBERSORTx	CIBERSORTx (stanford.edu)
ImageJ	National Institutes of Health	ImageJ (nih.gov)
Tscratch	Tscratch	Gebäck et al.,[53]

RESOURCE AVAILABILITY

Lead contact

Further information and requests about this study should be directed to and will be fulfilled by the lead contact, Navin Varadarajan (nvaradar@central.uh.edu).

Material availability

This study did not generate new unique reagents.

Data and code availability

- Single-cell RNA-seq data have been deposited at GEO (GSE211561) and are publicly available as of the date of publication. Accession numbers are listed in the key resources table.
- This paper does not report original code.
- Any additional information required to reanalyze the data reported in this paper is available from the lead contact upon request.

EXPERIMENT MODEL AND SUBJECT DETAILS

Cell line

MDAMB231, HCC70, and MCF7 cells were purchased from ATCC. We cultured MDAMB231 and HCC70 cells in RPMI 1640 supplemented with 10% FBS, 1% L-glutamine, 1 % HEPES, and 1% penicillin-streptomycin.

We cultured MCF7 cells in Eagle's Minimum Essential Medium with 10% FBS, 1% HEPES, MEM Non-Essential Amino Acids, and penicillin-streptomycin. We tested all cells for mycoplasma contamination using real-time PCR.

METHOD DETAILS

Single-cell EV detection assay

We analyze the secretion of EVs from single cells as previously described.[26] Briefly, we labeled cells with PKH67 dye (Sigma-Aldrich, Cat. PKH67GL-1KT) as directed by the manufacturer. To capture the EVs on the surface of LumAvidin beads (Luminex, Cat. L100-L115-01), we incubated the beads with 3.5 μg/ml biotinylated anti-CD81 antibody (BioLegend, clone TAPA-1) at the room temperature for 40 min, followed by three washes in PBS with 1% BSA. Then we loaded the labeled cells and functionalized beads into nanowells coated with PLL-g-PEG (SuSoS) and incubated at 37 °C. At 45 min before each detection time point, we added 4 μg/ml PE-labeled anti-CD63 antibody (BioLegend, clone H5C6). We imaged the nanowell using Zeiss Axio Observer Z1 microscope equipped with 20x/0.8 NA objectives and a Hamamatsu Orca Flash v2 camera.

We analyzed the TIFF images exported from the microscope as previously described.[26] Briefly, we segmented, quantified the cell to bead ratio, identified the cell to bead ratio of 1:1, and calculated the background-subtracted pixel values for identification of secreting and non-secreting cells. To analyze the dynamic of secretion from single cells, we detected the wells which maintained the 1:1 ratio during entire time course of the experiment. Then, based on a two-tailed t-test of the CD63 intensity per pixel, we selected a significant increase with p-value < 0.01 as the criterion for a change in the secretion behavior of the cell.

Establishment of clonal cell lines

As previously described,[26] we used the CellCelector micromanipulator (ALS) equipped with 50-μm glass capillaries to retrieve the detected secretor and non-secretor single cells. Briefly, we profiled the secretion of EVs from single MDAMB231 cells within 6 hours. Once we identified the secreting and non-secreting single cells, we transferred the array to CellCelector and retrieved single cells in an automated manner. For each retrieval, the total amount of aspiration by the capillary was 1 μl consist of 0.3 μl complete media (before retrieving) and 0.7 μl from each single well (during retrieval). We transferred the retrieved cells to wells of a 96-well plate containing 200 μl complete media and cultured the cells up to 24 population doublings.

EV isolation and nanosight analysis

We collected 5 mL of culture media from the cells of interest and centrifuged at 3,000 x g for 15 minutes. The supernatant was collected and incubated with ExoQuick-TC (System Biosciences, Cat. EQULTRA-20TC-1) overnight at 4°C. The samples were centrifuged at 3,000 x g for 10 minutes and the supernatant was discarded. The pellet was resuspending in 200 μl of Buffer B from the kit.

The purified EV solution was diluted in PBS at a 1:100 dilution and was injected onto the NanoSight stage (Malvern Panalytical Nanosight LM14). After 15 minutes of settling, the EV solution was imaged for 768 frames for 5 separate runs. The output was analyzed using the Nanoparticle Tracking Analysis software v.2.3 to determine average EV size.

Wound healing assay

We cultured MDAMB231-S and MDAMB231-NS cells to 90% confluency in 12-well plates in media containing 10% FBS. We then replaced the media with media containing 0.5% FBS and cultured for an additional 18 h. After this starvation period, we scratched the monolayer with 10 μl pipette tips and washed the wells twice with PBS. During the assay, we incubated the cells with media containing 0.5% FBS. For the assays with EVs of MDAMB231-S and MDAMB231-NS, we incubated the cells with media containing 0.5% FBS and $8x10^8$ particles/ml of EVs. At several time points, we obtained images with the Zeiss Axio Observer Z1 microscope equipped with 20x/0.5 NA objectives. We analyzed the images with the Tscratch tool.[53]

EV quantification using a transwell assay

We utilized a Transwell insert with a 3-μm pore membrane. and loaded functionalized beads in the lower compartment, and cells in the upper compartment of the insert. For HSP90 inhibitor assays, we covered the transwell with 10 nM or 30 nM of tanespimycin or ganetespib. After 48 h at 37 °C, we collected the beads and labeled them with 4 μg/ml PE-labeled anti-CD63 antibody (BioLegend, clone H5C6) for 45 min at 37 °C. We subsequently washed the beads three times in PBS with 1% BSA and imaged the wells using a Zeiss Axio Observer Z1 microscope equipped with 20x/0.8 NA objectives. Using ImageJ, we segmented and measured the fluorescent intensity of CD63.

Surface marker staining

To measure the expression of CD81, we coated the cells with 3.5 μg/ml biotinylated anti-CD81 (BioLegend, clone TAPA-1) antibody at the 37 °C for 30 min. After one wash in PBS with 1% BSA, we stained the cells with 4 μg/ml PE-streptavidin (BioLegend) at the 37 °C for 45 min. We imaged the cells using a Zeiss Axio Observer Z1 microscope equipped with 20x/0.8 NA objectives, and quantified the CD81 signal using ImageJ.

Western blot methods

Cell lysates were extracted using 1x RIPA buffer (Millipore Sigma, Cat. 20-188) and 1x protease inhibitor cocktail (ThermoScientific, Cat. 1862209) in deionized water. The protein concentrations of the cell lysates were determined using the Pierce BCA Assay Kit (ThermoScientific, Cat. 23227). The proteins were incubated with 4x Laemmli sample buffer (BioRad, Cat. 1610747) and 2-mercaptoethanol (Sigma Life Science, Cat. M3148-20ML). The samples were boiled at 95°C for 5 minutes and cooled at room temperature for 15 minutes. 25 μg of the samples were loaded onto a pre-cast 4-15% polyacrylamide gel (BioRad, Cat. 4561084) with 1x tris/glycine/SDS (J.T Baker, Cat. 4109-02/ VWR Life Science, Cat. 56-40-6/ Hoefer, Cat. 151-21-3) running buffer. The gel ran for 90 minutes at 100 volts via vertical electrophoresis. The contents from the gel were transferred to a polyvinylidene fluoride (PVDF) membrane (Amersham Hybond, Cat. 10600023) membrane in 1x tris/glycine/methanol (J.T Baker, Cat. 4109-02/ VWR Life Science, Cat. 56-40-6/ BDH Chemicals, Cat. 67-56-1) transfer buffer at 90 volts for 60 minutes. The PVDF membrane was placed in a blocking buffer of 5% skim milk in 1x tris-buffered saline/TWEEN20 (TBST) (J.T Baker, Cat. 4109-02/ Fisher Bioreagents, Cat. BP358-212/ SIGMA, Cat. P7949-500ML) buffer for 2 hours. The membrane was then incubated overnight with rabbit monoclonal anti-HSP90alpha antibody (Clone D1A7, CST Cat. 8165S) in a solution of 2.5% bovine serum albumin (BSA) (Fisher Bioreagents, Cat. BP1600-100) in TBST. The membrane was washed three times for 10 minutes with TBST then incubated with anti-rabbit IgG HRP-conjugated antibody (Jackson ImmunoResearch, Cat. 111-035-144) in 2.5% BSA in TBST for 60 minutes. The membrane was washed three times with TBST and developed using Pierce 1-Step Ultra TMB Blotting Solution (ThermoScientific, Cat. 37574). The loading control was identically prepared; the primary antibody used was anti-β-actin antibody (Clone 2F1-1, Biolegend Cat. 643802) and the secondary antibody was anti-mouse IgG HRP-linked antibody (CST, Cat. 7076S). Images were taken via cellular device.

Single-cell RNA-sequencing

We labeled HCC70, MCF7, MDAMB231, MDAMB231-S, and MDAMB231-NS cells separately with the Sample-Tags from the BD Human Immune Single-Cell Multiplexing Kit (BD Biosciences) as described in the manufacturer's protocol. Then, we prepared a library from ~5000 cells (approximately 1000 cells from each group). We used the BD Rhapsody System to prepare samples for transcriptome analysis. We assessed the quality and quantity of the final library using the Agilent 4200 TapeStation system using the Agilent High Sensitivity D5000 ScreenTape and a Qubit dsDNA HS Assay, respectively. We diluted the final library to 3 nM concentration and used a HiSeq PE150 sequencer (Illumina) to perform the sequencing.

QUANTIFICATION AND STATISTICAL ANALYSIS

All data presented represent mean ± SEM, unless mentioned. Analyses were carried out in GraphPad Prism (v6.0). Two-tailed t-test was performed between two groups, unless indicated otherwise. We considered p value < 0.05 as a significant threshold for comparisons, unless indicated otherwise.

Sequencing read alignments

We analyzed the FASTQ files using the BD Rhapsody WTA Analysis Pipeline available on the Seven Bridges website (https://www.sevenbridges.com/). After performing alignment, filtering, and sample tag detection, we downloaded the sample tag calls and molecule count information for further analysis in R (v 4.0.1) using Seurat Package (v 3.0).[54]

Data processing and identification of differentially expressed genes

We performed the clustering using the standard processing workflow in the Seurat Package. Briefly, we removed cells with less than 8000 gene count, cells with mitochondrial genes at greater than 20% of the reads, and cells in clusters that contained a mixture of sample tags, resulting in 3431 single-cell profiles (773 MDAMB231-S cells, 815 MDAMB231-NS cells, 971 MDAMB231 cells, 645 MCF7 cells, and 227 HCC70 cells). Next, we identified the differentially expressed genes using the *Findmarkers* function in Seurat. We selected the markers with greater than 1.2-fold higher expression in MDAMB231-S cells in comparison to MDAMB231-NS cells as the gene signature for EV secretion.

ExoCarta dataset analysis

We downloaded the list of proteins and mRNAs in the ExoCarta dataset http://exocarta.org/download.

Gene correlation analysis

To calculate the Spearman correlation between genes, we used the *cor.test* function in R. We created the heatmaps of correlation coefficients with *pheatmap* package (v 1.0.12).

Gene set enrichment analysis for breast cancer cell lines

To perform pathway analysis, we pre-ranked DEGs (p-value < 0.05) between each pair of cell lines identified using the *Findmarkers* function in *Seurat* package. We ran the GSEA software provided by UC San Diego and Broad Institute using Broad Institute C2: curated gene sets.

Core signature identification and network analysis

We calculated the Spearman correlations between identified DEGs between MDAMB231-S cells and MDAMB231-NS cells. We used *ward.D2* as a hierarchal clustering method along with *Euclidean* distance method to cluster the markers. Using the *pvclust* package (v 2.2-0),[55] we assessed the uncertainty in clustering analysis. We used the approximately unbiased value > 95 as the criteria for a significant cluster. We plotted the heatmap using *pheatmap* package.

To build the network between markers, we used *igraph* package (v 1.2.5).[56] First, we created an undirected network containing a list of links and nodes. The size of nodes represented the average gene expression of each marker and the links represented the Spearman coefficient between each marker. Next, we removed the negative links, and to simplify the network, we removed the links that showed a smaller coefficient than the average of positive links. To visualize the network, we used the layout algorithm of layout_with_graphopt.

Cancer cell line encyclopedia (CCLE) analysis

We downloaded the CCLE log2 transformed RNA-seq TPM gene expression and the cell line information from the DepMap portal (https://depmap.org/portal/download/). To perform the correlation analysis, we filtered the gene expression matrix for the genes of EV-sig and determined Spearman correlations among these genes in the 1304 cell lines available. To analyze the correlations with respect to breast cancer subtype, we first selected breast cancer cell lines using the *primary_disease* information. Then, using the *lineage_molecular_subtype*, we grouped the cell lines into different subtypes.

TCGA and METABRIC analyses

We downloaded all the TCGA data, including raw counts, RSEM gene normalized expression, and clinical data from the Broad Institute FireBrowse Data Portal (www.firebrowse.org). For tumor size, and stage analyses, we downloaded the *BRCA_clinicalMatrix* file from University of California Santa Cruz Xena Hub Portal (https://xena.ucsc.edu/) and used *PAM50_mRNA_nature2012*, *Tumor_nature2012*, and *AJCC_Stage_nature2012* for PAM50, tumor size, and stages information, respectively. We downloaded all

METABRIC data, including gene expression and clinical data from the cbioportal for cancer genome (www.cbioportal.org). We calculated the Spearman's rank correlation coefficients using the *cor.test* function and plotted using *pheatmap* package in R. For survival analysis, we used the Kaplan-Meier method. We compared the overall survival of patients divided by the median expression of the four EV-sig genes. Using the log-rank test, we calculated the statistical significance of survival curves. To perform pathway analysis, we identified DEGs between patients and divided by the median expression of the four EV-sig genes using the *DESeq2* (v 1.22.2) package[57] for TCGA dataset. To calculate the DEGs for the METABRIC dataset, we performed a Wilcoxon test. We next used the pre-ranked genes with a significant *p*-value of < 0.05 to run GSEA software provided by UC San Diego and Broad Institute using Broad Institute C2: curated gene sets. We used the normalized gene expression of breast cancer patients to estimate the relative fraction of 22 immune cell types using 1000 permutations with the CIBERSORTx analytical tool. We calculated the cytolytic activity as the geometric mean of *PRF1* and *GZMA* as previously described.[58]

scRNA-seq analysis of primary tumors

We downloaded the matrix of gene counts, features, and barcodes of two datasets, GSE176078 [59] and GSE180286,[60] from the NCBI repository. We uploaded files into R (v 4.0.1) and processed them using Seurat Package (v 3.0). To filter out the cells from GSE176078, we selected cells with a gene and unique molecular identifier count greater than 200, and 250, respectively, and a mitochondrial percentage less than 20%. To filter out the cells from GSE180286, we selected cells with a gene and unique molecular identifier count greater than 100, and 200, respectively, and a mitochondrial percentage less than 50%. We used Seurat (v.3.0) to perform data normalization, data integration, dimensionality reduction, and clustering using default parameters. The clusters of epithelial cells were identified by expression of *EPCAM*. We classified the ER^+ or $HER2^+$ patients as Non-TNBC patients. We used AUCell[61] (v 1.10) method to calculate the EV score for every single cell based on the expression of EV-sig genes.